This is a repository copy of *Path-dependent initialization of a single quantum dot exciton spin in a nanophotonic waveguide*.

White Rose Research Online URL for this paper:
http://eprints.whiterose.ac.uk/114170/

Version: Supplemental Material

Article:
Coles, R.J., Price, D.M., Royall, B. et al. (4 more authors) (2017) Path-dependent initialization of a single quantum dot exciton spin in a nanophotonic waveguide. Physical Review B, 95 (12). 121401(R) . ISSN 2469-9950

https://doi.org/10.1103/PhysRevB.95.121401

© 2017 American Physical Society. This is an author produced version of a paper subsequently published in Physical Review B, 95, 121401(R). Uploaded in accordance with the publisher's self-archiving policy.

Reuse
Items deposited in White Rose Research Online are protected by copyright, with all rights reserved unless indicated otherwise. They may be downloaded and/or printed for private study, or other acts as permitted by national copyright laws. The publisher or other rights holders may allow further reproduction and re-use of the full text version. This is indicated by the licence information on the White Rose Research Online record for the item.

Takedown
If you consider content in White Rose Research Online to be in breach of UK law, please notify us by emailing eprints@whiterose.ac.uk including the URL of the record and the reason for the withdrawal request.

eprints@whiterose.ac.uk
https://eprints.whiterose.ac.uk/

Supplemental material for path-dependent initialisation of a single quantum dot exciton spin in a nanophotonic waveguide

R.J. Coles,[1] D.M. Price,[1] B. Royall,[1] E. Clarke,[2] M.S. Skolnick,[1] A.M. Fox,[1,*] and M.N. Makhonin[1,†]

[1] *Department of Physics and Astronomy, University of Sheffield, Sheffield, S3 7RH, UK.*
[2] *EPSRC National Centre for III-V Technologies, Department of Electronic and Electrical Engineering, University of Sheffield, Sheffield S1 3JD, UK*

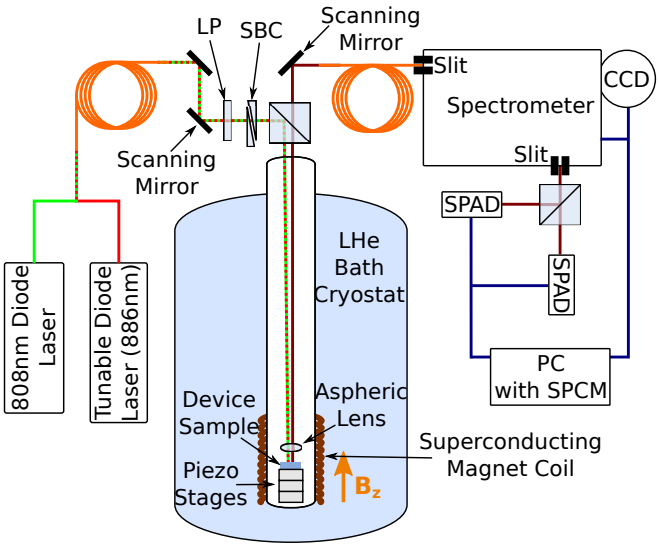

FIG. S1. Schematic diagram of the experimental apparatus. LP=Linear polarizer, SBC=Soleil-Babinet Compensator, CCD=Charge Coupled Device Camera, SPAD= Single Photon Avalanche Diode, SPCM=Single Photon Counting Module.

SAMPLE DETAILS AND EXPERIMENTAL SETUP

The samples were grown by molecular beam epitaxy on an undoped GaAs (100) wafer, comprising a 140 nm GaAs membrane with a single layer of InGaAs Quantum dot (QDs) at its centre, above a 1 μm sacrificial $Al_{0.6}Ga_{0.4}As$ layer on an undoped GaAs substrate. The waveguide devices were fabricated by electron beam lithography followed by an inductively coupled plasma etch through the GaAs membrane. The sacrificial $Al_{0.6}Ga_{0.4}As$ layer was removed by an isotropic HF acid etch to leave a free-standing waveguide. To confine only the single, fundamental TE-like mode to the waveguide the lateral dimensions used were 140×280 nm which correspond to $\lambda/2n \times \lambda/n$. This rectangular cross section breaks the degeneracy between TE and TM modes, and ensures maximal confinement of the TE mode. The waveguides were 15 μm long with $\lambda/2n$ semicircular grating couplers at each end [1].

A schematic of the experimental setup is shown in Fig. S1. The sample is held at 4.2 K in a liquid helium bath cryostat and a magnetic field B_z is applied normal to the device plane using a superconducting magnet coil. QD photoluminescence (PL) was excited using an above GaAs bandgap 808 nm diode laser and/or a single mode diode laser tuned to a p-shell resonance of the QD. The polarization of the tunable laser was controlled using a motorized linear polarizer and a Soleil-Babinet compensator (SBC). A confocal microscopy system with two motorized scanning mirrors allows for independent spatial control of quasiresonant and nonresonant excitation lasers, and of PL detection. Both excitation and PL detection were through the same 0.5 NA focussing aspheric lens. A 0.75 m spectrometer with 1800 lines/mm grating diffracts the light onto a charge coupled device camera (CCD) to record PL spectra, whilst the same spectrometer also filters PL emission for detection with single-photon avalanche photodiodes (SPADs). Hanbury-Brown Twiss measurements were performed using a beamsplitter after the spectrometer with a SPAD in each output path, where a computer containing a single photon counting module interfaced with the SPADs records the time-correlated single-photon detection events.

IDENTIFICATION OF QD WITH HIGH CHIRAL CONTRAST

Selection of a QD, from a randomly positioned ensemble, which exhibits undirectional emission was first conducted using PL spectroscopy with nonresonant (NR) laser diode excitation at 808 nm under an applied magnetic field of $B_z = 1$ T. This is shown schematically in Fig. S2(a). The magnetic field lifts the degeneracy of the spin eigenstates of the QD exciton through the Zeeman effect and facilitates their identification via emission of circularly polarized photons of different wavelength. Figure S2(b) shows PL spectra of a chirally-coupled QD when detecting PL emission from the grating couplers. Strong emission from respective Zeeman components (σ^+/σ^-) is observed from each grating (left/right) with Zeeman energy splitting $\Delta E_z = 147$ μeV. The spin readout contrast is derived as in [2] from the relative integrated

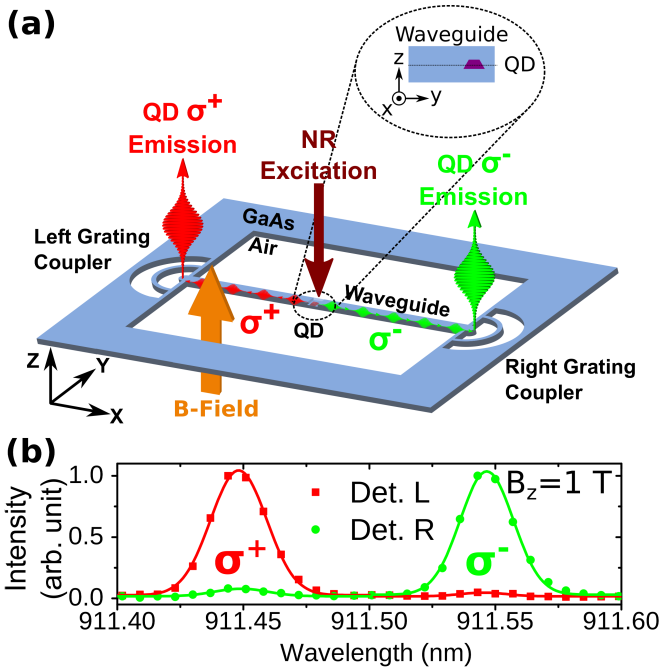

FIG. S2. (color online). (a) Schematic of the device structure and experimental arrangement for QD exciton spin readout. A cross section of the waveguide indicating the QD location within the waveguide. (b) PL spectra of the chirally coupled QD taken at $B_z = 1$ T when detecting emission from each of the two grating couplers (left,right labelled and shown with corresponding color).

intensity of the Zeeman components $I^{\sigma+}$ and $I^{\sigma-}$ using

$$C^{read}_{det.l/r} = \frac{I^{\sigma+}_{l/r} - I^{\sigma-}_{l/r}}{I^{\sigma+}_{l/r} + I^{\sigma-}_{l/r}}, \tag{S1}$$

where the subscripts l/r refer to the left and right coupler from which PL emission is detected. Readout contrasts of $C^{read}_{det.l} = 0.95 \pm 0.05$ and $C^{read}_{det.r} = -0.88 \pm 0.06$ are observed from the left and right couplers respectively. These reduced readout contrasts compared to the initialisation contrasts presented in the main text are attributed to longer duration spin memory under QR excitation. The small discrepancy in contrasts between left and right detection may arise from a slight asymmetry in the reflectivity of the grating couplers due to fabrication imperfections. From FDTD simulations we estimate that the coupling efficiency of circularly polarized PL emission from the QD to the waveguide mode propagating in one direction is 68% and 0% in the reverse direction at a C-point [2].

IDENTIFICATION OF X^+ EMISSION

The PL spectrum of the QD studied in the main text under nonresonant (NR) excitation is shown in Fig. S3,

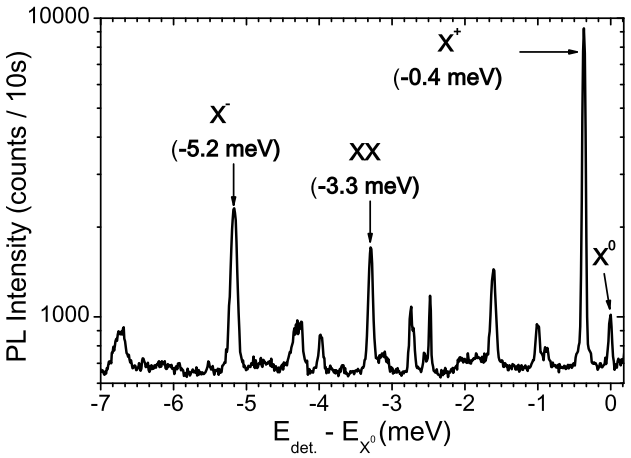

FIG. S3. PL spectrum of the QD under NR excitation of power $P_{NR} = 500$ nW. Excitonic species are labelled according to their energy separation from the neutral exciton, X^0. Other spectral lines arise either from spatially adjacent QDs in the waveguide or additional unidentified transitions within the same QD. The horizontal axis plots the difference between the detection and X^0 emission energy.

where the X^0 and XX states were identified from their relative power dependences. The emission line under study in the main text is attributed to positively charged exciton recombination ($X^+ \rightarrow h^+$) since it has no detectable fine structure splitting and occurs 0.4 meV below the X^0 recombination energy, consistent with the energy range for X^+ recombination [3, 4] (X^- is typically 5-7 meV to lower energy [5]). Indeed, the relative energies of the various excitonic species in Fig. S3 are in very good agreement with those presented in [3, 4]. Furthermore, for p-shell excitation, the X^+ line is only observed in the presence of additional NR excitation which creates the resident hole in the QD, further consistent with its attribution.

The spin states of X^+ are $|\downarrow\Uparrow\Downarrow\rangle$ and $|\uparrow\Uparrow\Downarrow\rangle$, where $\uparrow,\downarrow$ and $\Uparrow,\Downarrow$ denote electron and heavy hole spins respectively. These states correspond to residual hole spin states $|\Downarrow\rangle$ and $|\Uparrow\rangle$ where σ^+ and σ^- photons are emitted, on exciton recombination, to the left and right waveguide directions correspondingly.

IDENTIFICATION OF P-SHELL RESONANCE

Identification of the p-shell resonance was conducted using a photoluminescence excitation (PLE) experiment. A weak (~ 10 nW) 808 nm laser was applied to the QD in the waveguide to create the additional hole for the $X^+ \rightarrow h^+$ transition and to stabilize the charge state of the QD. A tunable single mode diode laser (~ 650 nW) was applied to the left grating coupler and PL was collected from the right grating coupler. The tunable laser was tuned over 880-890 nm and the integrated intensity

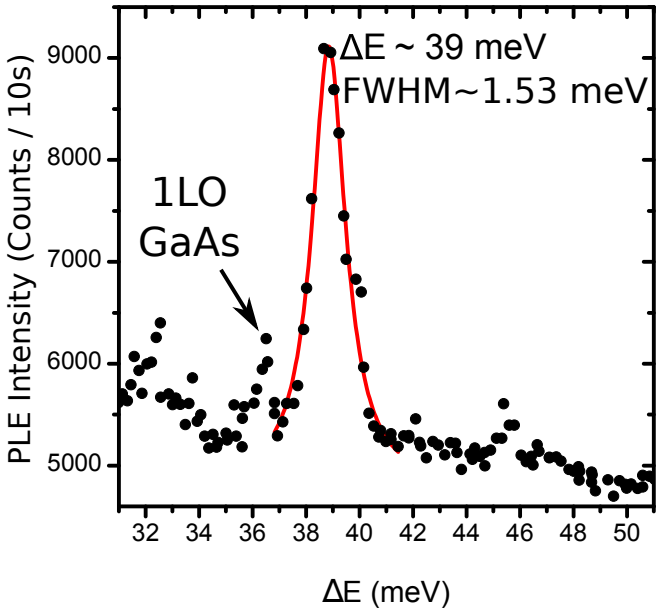

FIG. S4. PLE spectrum of the QD at the chiral point in the waveguide. The horizontal axis plots the energy difference between the laser excitation energy and detection at the X^+ emission energy. A strong p-shell resonance is observed at $\Delta E = E_{exc.} - E_{det.} = 39$ meV with linewidth ∼1.53 meV.

of the QD PL peak at 911.5 nm recorded at each wavelength step. The PLE spectrum is shown in Fig. S4(a), where a strong absorption peak is seen at a detuning from the ground state X^+ emission of 39 meV, in addition to the weaker bulk GaAs 1LO phonon resonance at 36.6 meV. By comparison with very similar results presented in [4], we attribute the intense peak at 39 meV to the p-shell resonance of the X^+ in which both the photogenerated electron and hole are in the p-shell excited states. The exciton then decays via fast LO phonon relaxation to the X^+ ground state, which accounts for its broad PLE linewidth of 1.53 meV. The phonon emission process conserves spin, so p-shell excitation preserves the initial spin of the excited state [4]. The linewidth of the p-shell absorption exceeds the Zeeman energy splitting of the X^+ transition at 1 T, $E_z = 147$ μeV. This enables both spin components to be efficiently prepared by appropriately polarized p-shell excitation.

HANBURY-BROWN TWISS MEASUREMENTS

The single photon characteristic of the QD emission under the QR excitation scheme presented in the main text was confirmed by Hanbury-Brown Twiss (HBT) measurements. We compare second order autocorrelation functions of the QD emission for both excitation schemes, NR and QR in Fig. S5(a) and Fig. S5(b) respectively. For NR excitation, the autocorrelation function $g^{(2)}(\tau)$ shows $g^{(2)}(0) = 0.06 \pm 0.04$. The autocorrelation function for QR excitation demonstrates a slightly higher value of $g^{(2)}(0) = 0.21 \pm 0.03$. The increased value in $g^{(2)}(0)$ under QR excitation is attributed to bunching due to charge fluctuation under QR excitation conditions, similar to that seen previously under resonant excitation [6]. These results confirm that the single photon character of the QD emission is maintained under QR excitation.

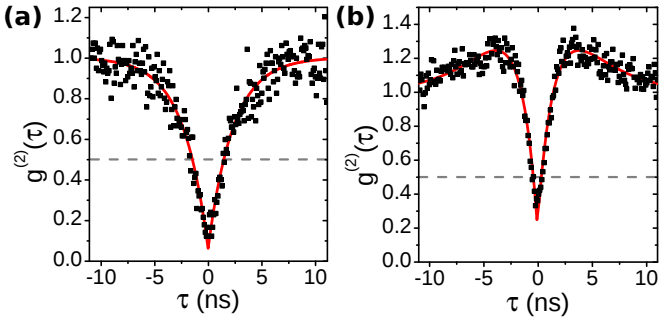

FIG. S5. (a) Autocorrelation function $g^{(2)}(\tau)$ for NR excitation, which exhibits $g^{(2)}(0) = 0.06 \pm 0.04$ and (b) autocorrelation function for QR excitation from the grating coupler yielding $g^{(2)}(0) = 0.21 \pm 0.03$. Raw data are plotted as discrete black points whilst fits to the data are shown as solid red lines.

POLARIZATION INDEPENDENCE OF SPIN INITIALISATION

The waveguide studied in this work confines a single TE-like optical mode with a fixed phase relationship between the transverse and longitudinal E-field components. The grating couplers couple this mode to the continuum of free space optical modes, where the polarization of the far fields of the coupler are inherited from the waveguide mode. The incoupling efficiency depends upon the overlap between the incoming laser and the free space modes of the grating, which in turn depends upon the laser polarization. However, once a laser photon is coupled to the waveguide mode, all memory of the input laser polarization is lost. Since the chiral coupling of the QD is determined by the local electric field polarization of the waveguide mode, the initialisation contrast is thus expected to be independent of the QR laser polarization. This behaviour is illustrated in Fig. S6, where raster scans of the QR laser of linear (H,V,D,AD) and left/right circular polarization are presented whilst keeping PL detection fixed on one grating coupler. These all demonstrate a high degree of spin initialisation contrast. All laser polarizations couple to the waveguide mode, but maximum efficiency is seen for transverse (V) polarization in Fig. S6(c)-(d) where a maximum PL intensity of ∼4700 counts is observed, whereas an average of ∼2300 counts is detected for the other polarizations. This is ex-

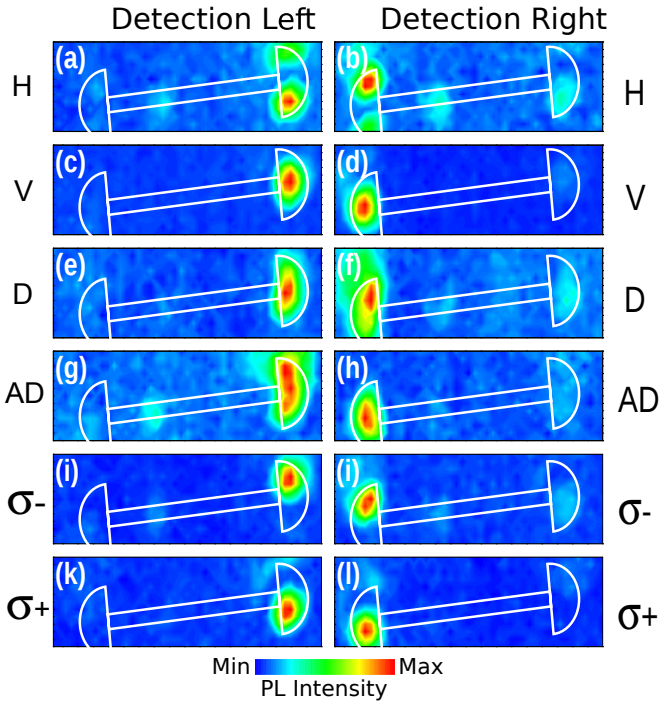

FIG. S6. Excitation maps obtained at $B_z = 0$ T using a raster scan of the quasiresonant laser over the device, filtered at the QD emission wavelength of 911.5 nm. The same laser powers were used in all scans. In the left and right columns the position of detection is fixed at the left and right grating coupler respectively, when the QR laser polarization is (a)-(b) horizontal, (c)-(d) vertical, (e)-(f) diagonal, (g)-(h) antidiagonal, (i)-(j) left circular, and (k)-(l) right circular. The polarizations are defined relative to the horizontal axis of the apparatus. A schematic outline of the waveguide and coupler is added in white. The apparent rotation of the devices is due to a small rotation induced by the detection optics.

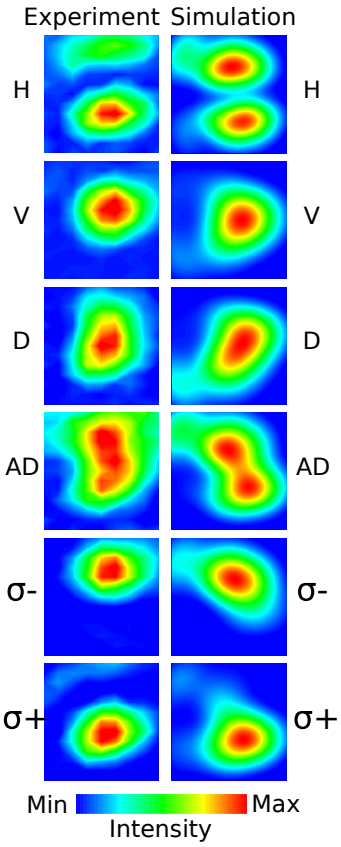

FIG. S7. (left column) Excitation maps over the right grating coupler when collecting PL emission from the left grating coupler for a range of laser polarizations. (right column) Simulated farfield profiles of scattered light from a grating coupler for a range of polarizations. In the simulated data, a convolution of the far fields of the grating coupler and a Gaussian beam is applied.

pected since the grating principally couples transversely polarized fields to the waveguide mode [6], so when the incoming laser is also transversely polarized the field overlap is maximized and the waveguide mode is excited with maximum efficiency. The polarization of the QR laser therefore determines the absolute intensity of the $\sigma^{+/-}$ PL emission peaks, but not their relative intensity.

FDTD simulations were performed to map the coupling efficiency of the grating couplers. A cross sectional modal field source in the waveguide emits into the waveguide mode, which is scattered out of the device plane by the coupler. A field monitor was positioned above the coupler which records the near fields. Analysis of the far field profiles was achieved using a near to far field transformation of the monitor field data within the software [7]. The comparison between experimental and simulation data is presented in Fig. S7 which shows the far field profiles of the grating couplers for experimental (left column) and simulated (right column) data. Good agreement is seen between the data which confirms the origin of the profiles of the PL map in Fig. S6. A slight deviation from simulation is observed for H polarization in experiment arises from poorer PL collection efficiency at large mirror deflections near the edge of the scanning window. polarization analysis was conducted, using Jones calculus, by calculating the transmitted intensity $|\mathbf{P}_{\theta,\phi}\mathbf{E}|^2$, where $\mathbf{E}$ is the electric far field vector and $\mathbf{P}_{\theta,\phi}$ is a polarization matrix given by:

$$\mathbf{P}_{\theta,\phi} = \begin{pmatrix} \cos^2\theta & \sin\theta\cos\theta e^{-i\phi} \\ \sin\theta\cos\theta e^{i\phi} & \sin^2\theta \end{pmatrix}. \qquad \text{(S2)}$$

Here, θ is the relative angle between the waveguide and the horizontal axis and ϕ is the circularity of the polarizer ($\phi = 0$ for linear and $\phi = \pm\pi/2$ for circular). To enable a realistic comparison between experiment and simulation, these data were convolved with a 2D spatial Gaussian function which approximates the laser beam profile with FWHM $\sim$1 μm.

The grating couplers principally scatter vertically polarized light at small angles and horizontally polarized light at large angles into two distinct cones. Therefore,

the farfield profiles for y-polarization show a single peak near the centre of the coupler whereas x-polarized fields show two distinct peaks either side of the coupler. For diagonal and antidiagonal polarization, a broader spot is seen which overlaps the y-polarized peak and one of the two x-polarized peaks. For circular polarization a peak is seen only above or below the centre of the grating coupler. This observation is due to the opposing phase of the longitudinal electric field components of the waveguide mode above and below the waveguide axis.

* mark.fox@sheffield.ac.uk
† m.makhonin@sheffield.ac.uk

[1] A. Faraon, I. Fushman, D. Englund, N. Stoltz, P. Petroff, and J. Vuckovic, Opt. Express **16**, 622 (2008).
[2] R. J. Coles, D. M. Price, J. E. Dixon, B. Royall, E. Clarke, P. Kok, M. S. Skolnick, A. M. Fox, and M. N. Makhonin, Nat. Commun. **7**, 11183 (2016).
[3] E. Poem, Y. Kodriano, C. Tradonsky, B. D. Gerardot, P. M. Petroff, and D. Gershoni, Phys. Rev. B **81**, 85306 (2010).
[4] Y. Benny, Y. Kodriano, E. Poem, D. Gershoni, T. A. Truong, and P. M. Petroff, Phys. Rev. B **86**, 085306 (2012).
[5] R. Warburton, C. Schaflein, D. Haft, F. Bickel, a. Lorke, K. Karrai, J. Garcia, W. Schoenfeld, and P. Petroff, Nature **405**, 926 (2000).
[6] M. N. Makhonin, J. E. Dixon, R. J. Coles, B. Royall, I. J. Luxmoore, E. Clarke, M. Hugues, M. S. Skolnick, and A. M. Fox, Nano Lett. **14**, 6997 (2014).
[7] Lumerical Solutions Inc., "Lumerical FDTD solutions," (2013).